JACS Au
AN OPEN ACCESS JOURNAL OF THE AMERICAN CHEMICAL SOCIETY

pubs.acs.org/jacsau
Letter

DNA Framework Programmed Conformational Reconstruction of Antibody Complementary Determining Region

Liqi Zhou, Lei Ren, Zhiang Bai, Qinglin Xia, Yue Wang, Hongzhen Peng, Qinglong Yan, Jiye Shi, Bin Li, Linjie Guo,* and Lihua Wang*

Cite This: JACS Au 2023, 3, 2709−2714

Read Online

ACCESS | Metrics & More | Article Recommendations | Supporting Information

ABSTRACT: The conformation of complementary determining region (CDR) is crucial in dictating its specificity and affinity for binding with an antigen, making it a focal point in artificial antibody engineering. Although desirable, programmable scaffolds that can regulate the conformation of individual CDRs with nanometer precision are still lacking. Here, we devise a strategy to program the CDR conformation by anchoring both ends of a free CDR loop to specific sites of a DNA framework structure. This method allows us to define the span of a single CDR loop with an ∼2 nm resolution. Using this approach, we create a series of DNA framework based artificial antibodies (DNFbodies) with varied CDR loop spans, leading to different antibody−antigen binding affinities. We find that an optimized single CDR loop (∼2.3 nm span) exhibits ∼3-fold improved affinity relative to natural antibodies, confirming the critical role of the CDR conformation. This study may inspire the rational design of artificial antibodies.

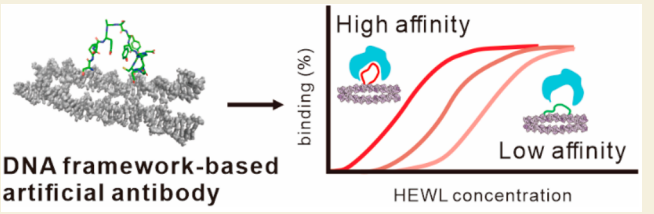

KEYWORDS: *DNA nanotechnology, artificial antibody, complementary determining region, conformation engineering, antibody−antigen binding affinity*

INTRODUCTION

Creating artificial antibodies with customizable properties yet high affinity against specific targets is desirable for a wide range of applications, such as biomedicine, bioimaging, and smart theranostics.[1,2] Antibodies are known to interact with antigens primarily through complementarity determining regions (CDRs) within the variable regions.[3] A CDR loop, typically comprising <20 amino acid residues, serves as the minimum motif to directly dictate the binding affinity with specific antigens through its amino acid sequence and 3D conformation.[4,5] Thus, CDR engineering has emerged as a key focus in artificial antibody development.[6−8] By grafting CDR loops onto engineered scaffold structures, one can adjust the CDR conformation, resulting in complexes with altered properties, such as antigen binding affinity, specificity, and stability.[9,10] For instance, the CDR conformation can be tuned by introducing site-directed mutagenesis in the scaffold proteins,[11−14] but the design freedom is constrained by protein structural conservation. Recently, an indirect approach for tuning CDR conformation has been reported, which relies on grafting CDRs onto synthetic nanoparticles with different densities.[15,16] A higher CDR density results in a shorter CDR span. However, the contribution of the CDR valency and CDR conformation to the antigen binding affinity can hardly be decoupled. Moreover, the typical CDR loop span is 1−2 nm, beyond the tuning resolution of most current synthetic materials. It is desirable yet challenging to construct programmable scaffolds allowing independent regulation of CDR conformation with a resolution at this size scale.[17]

DNA nanotechnology, leveraging Watson−Crick base pairing, allows for programmable design and synthesis of DNA nanostructures with precise sizes and shapes.[18−20] These structures, featuring B-form double-helix motifs with 2 nm diameter and ∼0.34 nm base pair spacing, provide scaffolds for moiety placement with subnanometer resolution.[21−25] This precise addressability has led to the use of DNA nanostructures as frameworks to organize proteins such as antibodies,[26,27] enzymes,[28,29] or their subunits,[30,31] enabling control over their quantities, combinations, interspaces, and orientations, thus regulating their activities and promoting biological applications.[32−34]

Here, we construct DNA framework based artificial antibodies (DNFbodies) with controlled CDR conformation by precisely dictating the anchoring distance of the CDR loop terminals on the DNA frameworks with ∼2 nm resolution. We investigate the relationship between the CDR loop span and antigen binding affinity. We successfully reconstruct an optimized CDR conformation exhibiting a 3-fold increase in

Received: August 22, 2023
Revised: September 18, 2023
Accepted: September 18, 2023
Published: September 28, 2023

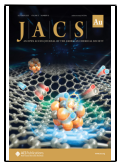

https://doi.org/10.1021/jacsau.3c00492
JACS Au 2023, 3, 2709−2714

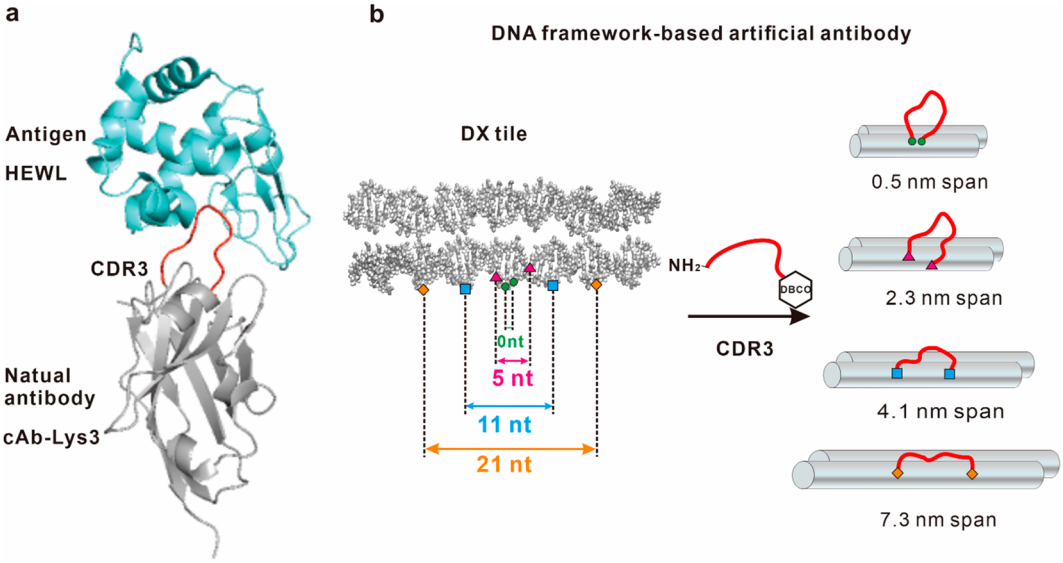

Figure 1. Scheme of the design of CDR grafting on DNA frameworks. (a) Structure of antibody cAb-Lys3 (gray, with the CDR3 loop shown in red) in complex with HEWL (cyan) (Protein Data Bank (PDB) ID code 1JTP). (b) Constructing DNA framework based artificial antibodies by anchoring a CDR3 loop modified with DBCO (dibenzocyclooctyne) and an amino group on DX tiles.

affinity compared to natural antibodies, effectively inhibiting lysozyme activity and showcasing its potential for practical applications.

RESULTS AND DISCUSSION

To reconstruct the CDR conformation, we used a double-crossover tile (DX tile) as the framework, known for its high rigidity.[35,36] Camelid antilysosome antibody (cAb-Lys3), consisting solely of a heavy chain, was selected as the natural

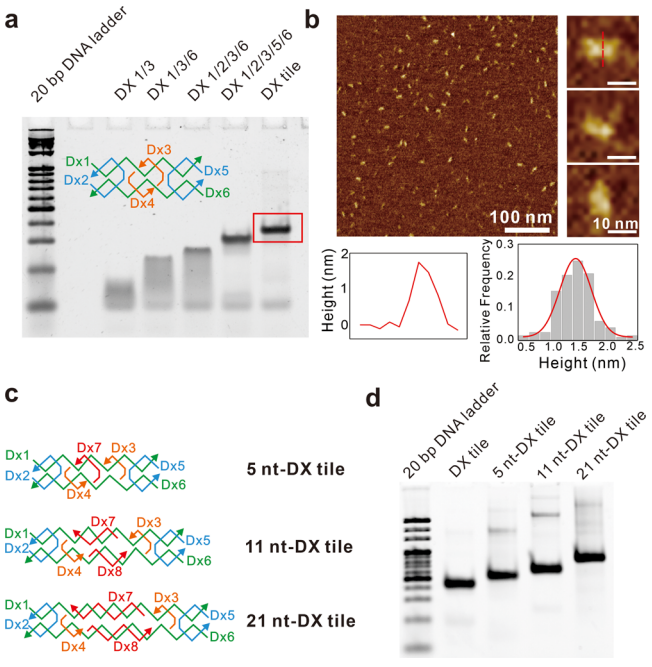

Figure 2. Synthesis and characterization of four DX tile structures. (a) Design and polyacrylamide gel electrophoresis (PAGE) of DX tile. (b) AFM images and height profile of DX tiles. (c) Schematic design of DX tiles with different spacers. (d) PAGE analysis of four DX tile structures.

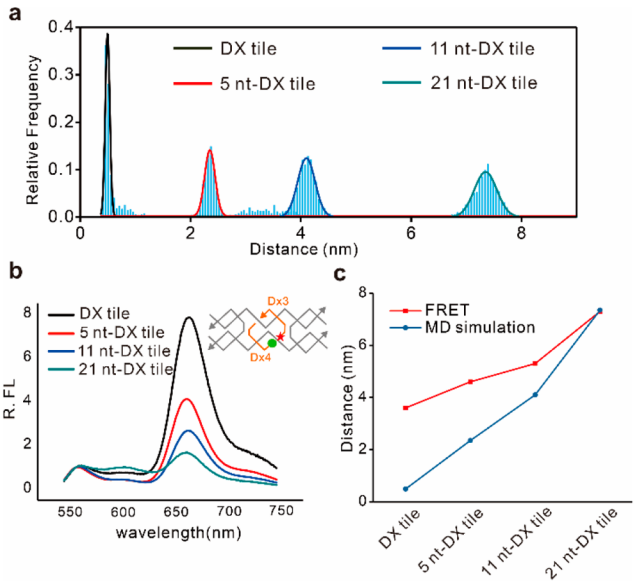

Figure 3. Spacing distance characterization of four DX tile structures. (a) Simulated distributions of spacing distance in DX tile, 5 nt-DX tile, 11 nt-DX tile, and 21 nt-DX tile (N = 1000). (b) Fluorescent spectra of DX tiles with FRET pair Cy3-Cy5. Excitation: 530 nm. Emission: 550−750 nm. (c) Distance comparison based on FRET and simulation.

antibody to be transformed into a DNA framework based artificial antibody (DNFbody). Crystallographic analysis of the cAb-Lys3/HEWL (hen egg white lysozyme) complex revealed that the N-terminal section of the CDR3 loop (comprising 100−112 amino acid residues) deeply extends into the active-site crevice of lysozyme, making most of the antigen contacts[37] (Figure 1a). Consequently, we chose the 13 amino acid residues spanning approximately 1.4 nm in the binding state for CDR3 grafting (Figure S1). In our experimental design, considering the structural stability of the DNA double helix and the interplay of complementary base pairing interactions,[38,39] we devised terminal spacing at intervals of 0, 5, 11,

https://doi.org/10.1021/jacsau.3c00492
JACS Au 2023, 3, 2709−2714

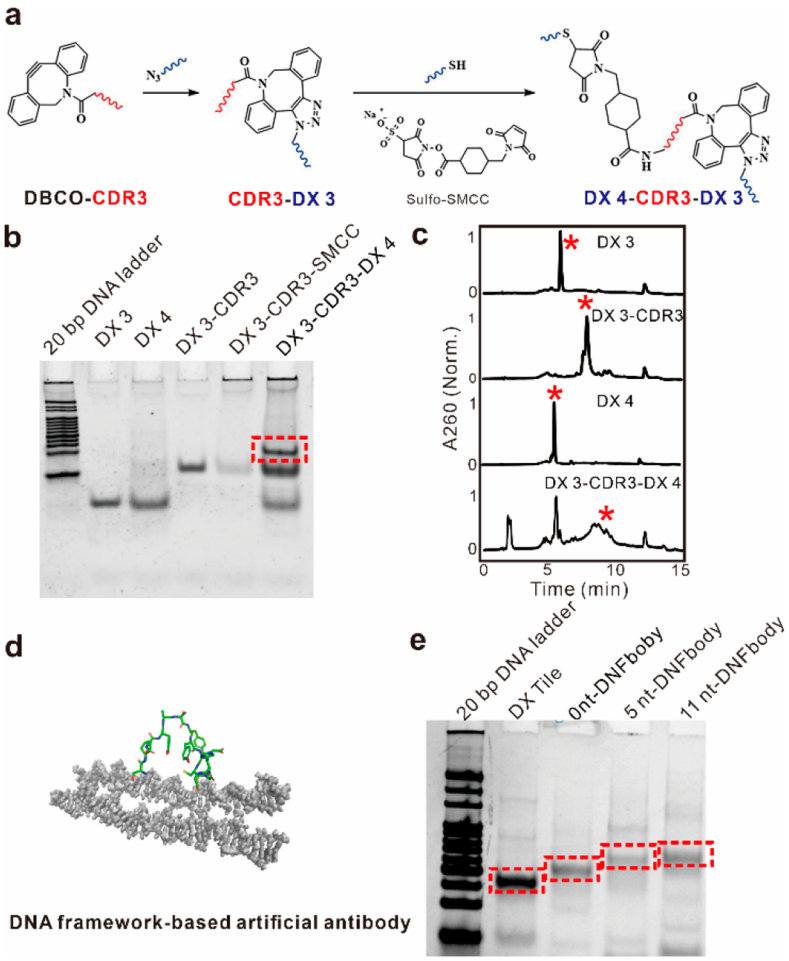

Figure 4. Synthesis and characterization of four DNFbodies. (a) CDR3 and DNA ligation mediated by click chemistry and SMCC. (b) Polyacrylamide gel electrophoresis (PAGE) of the CDR3-DNA conjugate (red dashed box). (c) High-performance liquid chromatography characterizing CDR3-DNA ligation (red star showing the main product). (d) Cartoon of DNFbody with a CDR3 loop anchored on a DNA framework. (e) PAGE analysis of DNFbodies and the DX tile.

and 21 nucleotides on DX tiles (Figure 1b). The two ends of the CDR3 loop were anchored to these predetermined locations through covalent conjugation. Based on this, we conducted research on the reconstruction of DNFbodies with varied CDR3 spans and their interaction with antigens.

First, DX tile (length 37 bp, or ∼12.6 nm, adapted from a previous study[40]) was assembled from six oligonucleotides (named DX 1−6, sequences listed in Supplementary Table). The synthesized structure was analyzed with polyacrylamide gel electrophoresis (PAGE). As shown in Figure 2a, we observed a sharp band of DX tile with the slowest migration compared to other structures partially assembled from 2 to 4 component oligonucleotides. Representative atomic force microscopy (AFM) images demonstrated efficient and uniform synthesis of the DX tile. The measured height distribution is 1.5 ± 0.5 nm, which matched the theoretical diameter of the double helix (Figure 2b and Figure S2). Meanwhile, we designed the other three DX tile structures (namely 5 nt-DX tile, 11 nt-DX tile, and 21 nt-DX tile), with the 5′-end of DX 3 and 3′-end of DX 4 separated by 5, 11, 21 spacer nucleotides, respectively (Figure 2c). The assembled structures were also confirmed by PAGE analysis (Figure 2d and Figure S3).

To assess the distance between predetermined locations in the DX tiles, we initially constructed coarse-grained models and conducted molecular dynamics (MD) simulations to examine their conformations in solution. The obtained simulation results (Figure 3a) reveal that the distance increases as the number of spacer nucleotides grows (0.5 ± 0.1, 2.3 ± 0.2, 4.1 ± 0.3, and 7.3 ± 0.4 nm for DX-Tile, 5 nt-DX tile, 11 nt-DX tile, and 21 nt-DX tile, respectively). For further verification of the distance between the 5′-end of DX 3 and the 3′-end of DX 4, we attached a Forster resonance energy transfer (FRET) pair of fluorescent molecules (Cy3 and Cy5) on either side of DX 3 and DX 4 (Figure 3b). Since FRET is dependent on the distance between the donor (Cy3) and acceptor (Cy5), the distance difference between the ends of DX 3 and DX 4 in the structures can be translated into variations of the fluorescence intensity.[41] From the fluorescence spectra in Figure 3b, it was observed that the fluorescent intensity of Cy5 (acceptor) was enhanced with a decrease in the designed distance, suggesting a distance-dependent FRET efficiency enhancement. The spacing distances calculated by FRET efficiency in DX tile, 5 nt-DX tile, 11 nt-DX tile, and 21 nt-DX tile were 3.6, 4.6, 5.3, and 7.3 nm, respectively, showing an increasing trend consistent with our design (Figure 3c). Overall, the calculated values match the simulated distances precisely in the case of the 21 nt-DX tile. However, the discrepancy emerges as the designed spacer

https://doi.org/10.1021/jacsau.3c00492
JACS Au 2023, 3, 2709−2714

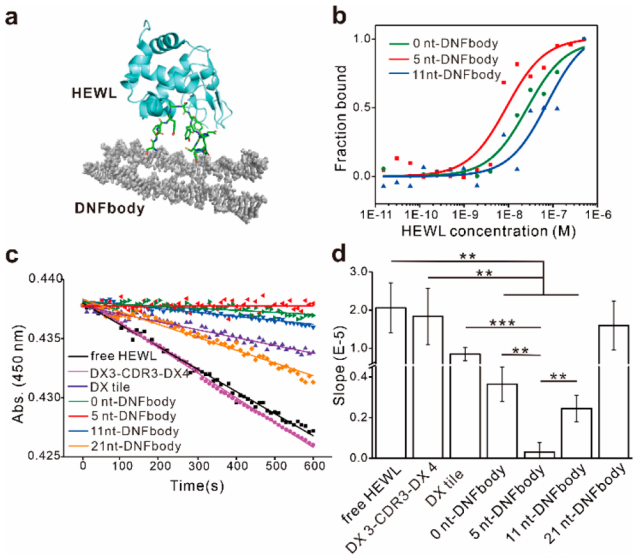

Figure 5. Interactions between DNFbody and HEWL. (b) MST analysis and fitting curves of the kinetics of the binding between the DNFbodies and HEWL. (c) Enzymatic activity assays of HEWL alone and in the presence of DX tile, DX 3-CDR3-DX 4 and four DNFbodies, respectively. (d) Statistical analysis of the slopes in the enzymatic activity assays. Representative data are expressed as mean ± SD. Student's *t* test was used to calculate statistical significance. ***$P < 0.001$, **$P < 0.01$.

decreases. This may be attributed to the introduction of the C6 chain for fluorescent molecule modification and the flexible oscillation of the two fluorescent molecules.

The CDR3 peptide was then designed to be grafted onto different DX tile structures. A Cys residue (C) was added at the C-terminal of CDR3 for maleimide-DBCO conjugation, which allows for a copper-free click reaction with azide-labeled DX 3. Then the N-terminal of CDR3 was covalently conjugated to sulfhydryl-modified DX 4 with the help of the heterobifunctional cross-linker SMCC (Figure 4a). The product of the CDR3-DNA conjugation was confirmed by PAGE and high-performance liquid chromatography (Figure 4b,c). Both the PAGE and HPLC results indicated that the yield of the conjugation (DX 3-CDR3-DX 4) was less than 100%. Consequently, the conjugation product intended for subsequent DNFbody synthesis was isolated and purified by PAGE. Subsequently, by annealing the purified CDR3-DNA conjugation product with the other constituent DNA strands of the DX tile, different DNFbodies were synthesized (Figure 4d). Depending on the specific DNA framework used, these DNFbodies were designated as 0 nt-DNFbody, 5 nt-DNFbody, 11 nt-DNFbody, and 21 nt-DNFbody, respectively. During PAGE analysis, the migration of bands corresponding to DNFbodies exhibited slower mobility in comparison to the bands of the DX tile alone (Figure 4e and Figure S4). This provides evidence that the CDR3 peptides were effectively immobilized onto the DX tiles.

After synthesis of a sequence of DNFbodies featuring diverse CDR3 conformations, an assessment was conducted to ascertain their specificity and affinity in binding to their antigen, HEWL (Figure 5a). First, the kinetics of the interaction between the DNFbodies and HEWL was assessed utilizing microscale thermophoresis (MST). The specific binding data obtained from MST was subjected to fitting using a 1:1 binding model. As depicted in Figure 5b, the fitting yielded dissociation constants (K_d) of 26.6 ± 7.3 nM for 0 nt-DNFbody, 8.5 ± 3.6 nM for 5 nt-DNFbody, and 64.9 ± 13.1 nM for 11 nt-DNFbody, which were found to be comparable to the original cAb-Lys3-HEWL interaction (20−50 nM).[42] The results revealed that all three DNFbodies exhibited the ability to bind to HEWL, with the 5 nt-DNFbody demonstrating the highest affinity to HEWL (~3-fold improvement compared to the natural antibody). Nevertheless, the MST data obtained for the 21 nt-DNFbody could not be adequately fitted into the binding model, indicating the absence of binding between the 21 nt-DNFbody and HEWL (Figure S5).

Given that the DNFbodies were specifically designed to bind to the active cleft of HEWL, quantification of the binding between DNFbodies and HEWL could be achieved by evaluating the inhibition of HEWL's bacteriolytic activity. Figure 5c shows the activity profiles of HEWL after incubation with different DNFbodies. The decreased slopes represent the inhibition of HEWL activity due to binding with different structures. It can be seen that DX 3-CDR3-DX 4 exhibits no impact on the activity of HEWL, implying that CDR3 could not bind to HEWL effectively without being attached to the DNF scaffold. Besides, the DX tile could partially inhibit the activity of HEWL due to the nonspecific protein adsorption of the DNA nanostructure.[43−45] DNFbodies featuring CDR3 conjugated on a DNA framework exhibited amplified inhibition of HEWL activity. The statistical analysis of the slope indicates that the four distinct DNFbodies exhibited varying degrees of inhibition against HEWL, with 5 nt-DNFbodies demonstrating the most efficient inhibition of HEWL activity (Figure 5d). These findings collectively provide evidence that diverse DNFbody structures exhibit varying spatial configurations of CDR3. Among these structures, 5 nt-DNFbody demonstrates the most favorable conformation for facilitating the optimal binding with HEWL, while 21 nt-DNFbody, due to its excessive terminal spacing, fails to adopt a conformation conducive to interacting effectively with the HEWL binding site.

CONCLUSION

In summary, we developed a novel approach to manipulate the conformation of antibody CDRs using DNA frameworks. We fabricated a series of DNA framework based artificial antibodies exhibiting varied binding affinity toward the antigen HEWL. This system has several advantages: first, compared to other CDR grafting methods, our approach offers higher spatial resolution for precise regulation of CDR loop span in the sub-10 nm range at a resolution of a single nucleotide. Second, DNA frameworks allow independent regulation of the CDR conformation, enabling the effect of the CDR conformation on antigen−antibody interactions to be decoupled from other factors including CDR valency. Moreover, individual DNFbodies can serve as modules to be assembled into larger structures through base pairing between the DX tiles, resulting in multivalent DNFbodies with a further improved antigen-binding affinity. Further, DNFbodies, which lack the Fc domain and are smaller in size compared with natural antibodies, have the potential to exhibit reduced adverse effects and improved tissue penetration. Consequently, they present promising prospects for applications in in vivo imaging and targeted drug delivery.

https://doi.org/10.1021/jacsau.3c00492
JACS Au 2023, 3, 2709−2714

■ ASSOCIATED CONTENT

Supporting Information

The Supporting Information is available free of charge at https://pubs.acs.org/doi/10.1021/jacsau.3c00492.

Materials, methods, polyacrylamide gel electrophoresis images, AFM images, MST analysis, and a table of DNA and peptide sequences (PDF)

■ AUTHOR INFORMATION

Corresponding Authors

Linjie Guo − *Institute of Materiobiology, College of Science, Shanghai University, Shanghai 200444, People's Republic of China*; Email: guolinjie@shu.edu.cn

Lihua Wang − *Institute of Materiobiology, College of Science, Shanghai University, Shanghai 200444, People's Republic of China; CAS Key Laboratory of Interfacial Physics and Technology, Shanghai Institute of Applied Physics, Chinese Academy of Sciences, Shanghai 201800, People's Republic of China; The Interdisciplinary Research Center, Shanghai Synchrotron Radiation Facility, Shanghai Advanced Research Institute, Chinese Academy of Sciences, Shanghai 201210, People's Republic of China*; Email: wanglihua@shu.edu.cn

Authors

Liqi Zhou − *National Laboratory of Solid State Microstructures, Jiangsu Key Laboratory of Artificial Functional Materials, College of Engineering and Applied Sciences and Collaborative Innovation Center of Advanced Microstructures, Nanjing University, Nanjing 210093, People's Republic of China; Institute of Materiobiology, College of Science, Shanghai University, Shanghai 200444, People's Republic of China*

Lei Ren − *Institute of Materiobiology, College of Science, Shanghai University, Shanghai 200444, People's Republic of China; CAS Key Laboratory of Interfacial Physics and Technology, Shanghai Institute of Applied Physics, Chinese Academy of Sciences, Shanghai 201800, People's Republic of China*

Zhiang Bai − *Institute of Materiobiology, College of Science, Shanghai University, Shanghai 200444, People's Republic of China*

Qinglin Xia − *Institute of Materiobiology, College of Science, Shanghai University, Shanghai 200444, People's Republic of China; CAS Key Laboratory of Interfacial Physics and Technology, Shanghai Institute of Applied Physics, Chinese Academy of Sciences, Shanghai 201800, People's Republic of China*

Yue Wang − *Institute of Materiobiology, College of Science, Shanghai University, Shanghai 200444, People's Republic of China; CAS Key Laboratory of Interfacial Physics and Technology, Shanghai Institute of Applied Physics, Chinese Academy of Sciences, Shanghai 201800, People's Republic of China*

Hongzhen Peng − *Institute of Materiobiology, College of Science, Shanghai University, Shanghai 200444, People's Republic of China*

Qinglong Yan − *Xiangfu Laboratory, Jiashan 314102, People's Republic of China*

Jiye Shi − *CAS Key Laboratory of Interfacial Physics and Technology, Shanghai Institute of Applied Physics, Chinese Academy of Sciences, Shanghai 201800, People's Republic of China*

Bin Li − *CAS Key Laboratory of Interfacial Physics and Technology, Shanghai Institute of Applied Physics, Chinese Academy of Sciences, Shanghai 201800, People's Republic of China; The Interdisciplinary Research Center, Shanghai Synchrotron Radiation Facility, Shanghai Advanced Research Institute, Chinese Academy of Sciences, Shanghai 201210, People's Republic of China*

Complete contact information is available at: https://pubs.acs.org/10.1021/jacsau.3c00492

Author Contributions

L.Z.: data curation, formal analysis, investigation, methodology, writing-original draft. L.R.: data curation, investigation, methodology. Z.B.: formal analysis, visualization. Q.X.: data curation, visualization. Y.W.: formal analysis. H.P.: investigation, methodology. Q.Y.: investigation, methodology. J.S.: funding acquisition. B.L.: project administration. L.G.: conceptualization, project administration, supervision, writing and editing. L.W.: resources, supervision, funding acquisition.

Notes

The authors declare no competing financial interest.

■ ACKNOWLEDGMENTS

This work was financially supported by the National Key R&D Program of China (2020YFA0908900), the China Postdoctoral Science Foundation (No. 2022M711564), and the Fellowship of China National Postdoctoral Program for Innovative Talents (No. BX2021119).

■ REFERENCES

(1) Brekke, O. H.; Sandlie, I. Therapeutic antibodies for human diseases at the dawn of the twenty-first century. *Nat. Rev. Drug. Discov.* **2003**, *2*, 52−62.

(2) Yu, H.; Liu, B.; Zhang, Y.; Gao, X.; Wang, Q.; Xiang, H.; Peng, X.; Xie, C.; Wang, Y.; Hu, P.; Shi, J.; Shi, Q.; Zheng, P.; Feng, C.; Tang, G.; Liu, X.; Guo, L.; Lin, X.; Li, J.; Liu, C.; Huang, Y.; Yang, N.; Chen, Q.; Li, Z.; Su, M.; Yan, Q.; Pei, R.; Chen, X.; Liu, L.; Hu, F.; Liang, D.; Ke, B.; Ke, C.; Li, F.; He, J.; Wang, M.; Chen, L.; Xiong, X.; Tang, X. Somatically hypermutated antibodies isolated from SARS-CoV-2 Delta infected patients cross-neutralize heterologous variants. *Nat. Commun.* **2023**, *14*, 1058.

(3) MacCallum, R. M.; Martin, A. C. R.; Thornton, J. M. Antibody-antigen interactions: Contact analysis and binding site topography. *J. Mol. Biol.* **1996**, *262*, 732−745.

(4) Dondelinger, M.; Filee, P.; Sauvage, E.; Quinting, B.; Muyldermans, S.; Galleni, M.; Vandevenne, M. S. Understanding the Significance and Implications of Antibody Numbering and Antigen-Binding Surface/Residue Definition. *Front Immunol.* **2018**, *9*, 2278.

(5) King, H. W.; Orban, N.; Riches, J. C.; Clear, A. J.; Warnes, G.; Teichmann, S. A.; James, L. K. Single-cell analysis of human B cell maturation predicts how antibody class switching shapes selection dynamics. *Sci. Immunol.* **2021**, *6*, No. eabe6291.

(6) Brekke, O. H.; Sandlie, I. Therapeutic antibodies for human diseases at the dawn of the twenty-first century. *Nat. Rev. Drug Discovery* **2003**, *2*, 52−62.

(7) Adams, G. P.; Weiner, L. M. Monoclonal antibody therapy of cancer. *Nat. Biotechnol.* **2005**, *23*, 1147−1157.

(8) Tsuchikama, K.; An, Z. Antibody-drug conjugates: recent advances in conjugation and linker chemistries. *Protein Cell.* **2018**, *9*, 33−46.

(9) Wu, A. M.; Senter, P. D. Arming antibodies: prospects and challenges for immunoconjugates. *Nat. Biotechnol.* **2005**, *23*, 1137−1146.
(10) Almagro, J. C.; Fransson, J. Humanization of antibodies. *Front. Biosci.* **2008**, *13*, 1619−1633.
(11) Oncu, M. D.; Balcioglu, B. K.; Ozgur, B.; Ozturk, H. U.; Serhatli, M.; Isik, S.; Erdag, B.; Doganay, G. D.; Bahadir, A. O. Structure-based engineering of an antiangiogenic scFv antibody for soluble production in E. coli without loss of activity. *Biotechnol. Appl. Bioc.* **2022**, *69*, 2122−2137.
(12) See, K.; Kadonosono, T.; Ota, Y.; Miyamoto, K.; Yimchuen, W.; Kizaka-Kondoh, S. Reconstitution of an Anti-HER2 Antibody Paratope by Grafting Dual CDR-Derived Peptides onto a Small Protein Scaffold. *Biotechnol. J.* **2020**, *15*, No. 2000078.
(13) Nicaise, M.; Valerio-Lepiniec, M.; Minard, P.; Desmadril, M. Affinity transfer by CDR grafting on a nonimmunoglobulin scaffold. *Protein Sci.* **2004**, *13*, 1882−1891.
(14) Dall'Acqua, W. F.; Damschroder, M. M.; Zhang, J.; Woods, R. M.; Widjaja, L.; Yu, J.; Wu, H. Antibody humanization by framework shuffling. *Methods.* **2005**, *36*, 43−60.
(15) Katz, E.; Willner, I. Integrated nanoparticle-biomolecule hybrid systems: synthesis, properties, and applications. *Angew. Chem., Int. Ed. Engl.* **2004**, *43*, 6042−6108.
(16) Yan, G. H.; Wang, K.; Shao, Z.; Luo, L.; Song, Z. M.; Chen, J.; Jin, R.; Deng, X.; Wang, H.; Cao, Z.; Liu, Y.; Cao, A. Artificial antibody created by conformational reconstruction of the complementary-determining region on gold nanoparticles. *Proc. Natl. Acad. Sci. U S A* **2018**, *115*, E34−E43.
(17) Tholen, M. M. E.; Rosier, B.; Vermathen, R. T.; Sewnath, C. A. N.; Storm, C.; Woythe, L.; Izquierdo-Lozano, C.; Riera, R.; van Egmond, M.; Merkx, M.; Albertazzi, L. Mapping Antibody Domain Exposure on Nanoparticle Surfaces Using DNA-PAINT. *ACS Nano* **2023**, *17*, 11665−11678.
(18) Seeman, N.; Sleiman, H. DNA nanotechnology. *Nat. Rev. Mater.* **2018**, *3*, 17068.
(19) Dey, S.; Fan, C.; Gothelf, K. V.; Li, J.; Lin, C.; Liu, L.; Liu, N.; Nijenhuis, M. A. D.; Saccà, B.; Simmel, F. C.; Yan, H.; Zhan, P. DNA origami. *Nat. Rev. Methods Primers.* **2021**, *1*, 13.
(20) Zhan, P.; Peil, A.; Jiang, Q.; Wang, D.; Mousavi, S.; Xiong, Q.; Shen, Q.; Shang, Y.; Ding, B.; Lin, C.; Ke, Y.; Liu, N. Recent Advances in DNA Origami-Engineered Nanomaterials and Applications. *Chem. Rev.* **2023**, *123*, 3976−4050.
(21) Ge, Z.; Gu, H.; Li, Q.; Fan, C. Concept and Development of Framework Nucleic Acids. *J. Am. Chem. Soc.* **2018**, *140*, 17808−17819.
(22) Jones, M. R.; Seeman, N. C.; Mirkin, C. A. Nanomaterials. Programmable materials and the nature of the DNA bond. *Science.* **2015**, *347*, No. 1260901.
(23) Jia, S.; Wang, J.; Xie, M.; Sun, J.; Liu, H.; Zhang, Y.; Chao, J.; Li, J.; Wang, L.; Lin, J.; Gothelf, K. V.; Fan, C. Programming DNA origami patterning with non-canonical DNA-based metallization reactions. *Nat. Commun.* **2019**, *10*, 5597.
(24) Yao, G.; Li, J.; Li, Q.; Chen, X.; Liu, X.; Wang, F.; Qu, Z.; Ge, Z.; Narayanan, R. P.; Williams, D.; Pei, H.; Zuo, X.; Wang, L.; Yan, H.; Feringa, B. L.; Fan, C. Programming nanoparticle valence bonds with single-stranded DNA encoders. *Nat. Mater.* **2020**, *19*, 781.
(25) Ouyang, X.; Wang, M.; Guo, L.; Cui, C.; Liu, T.; Ren, Y.; Zhao, Y.; Ge, Z.; Guo, X.; Xie, G.; Li, J.; Fan, C.; Wang, L. DNA Nanoribbon-Templated Self-Assembly of Ultrasmall Fluorescent Copper Nanoclusters with Enhanced Luminescence. *Angew. Chem., Int. Ed.* **2020**, *59*, 11836−11844.
(26) Ouyang, X.; De Stefano, M.; Krissanaprasit, A.; Kodal, A. L. B.; Rosen, C. B.; Liu, T.; Helmig, S.; Fan, C.; Gothelf, K. V. Docking of Antibodies into the Cavities of DNA Origami Structures. *Angew. Chem., Int. Ed.* **2017**, *56*, 14423−14427.
(27) Marcher, A.; Nijenhuis, M. A. D.; Gothelf, K. V. A Wireframe DNA Cube: Antibody Conjugate for Targeted Delivery of Multiple Copies of Monomethyl Auristatin E. *Angew. Chem., Int. Ed. Engl.* **2021**, *60*, 21691−21696.
(28) Li, S.; Jiang, Q.; Liu, S.; Zhang, Y.; Tian, Y.; Song, C.; Wang, J.; Zou, Y.; Anderson, G. J.; Han, J.; Chang, Y.; Liu, Y.; Zhang, C.; Chen, L.; Zhou, G.; Nie, G.; Yan, H.; Ding, B.; Zhao, Y. A DNA nanorobot functions as a cancer therapeutic in response to a molecular trigger in vivo. *Nat. Biotechnol.* **2018**, *36*, 258−264.
(29) Chen, Y.; Ke, G.; Ma, Y.; Zhu, Z.; Liu, M.; Liu, Y.; Yan, H.; Yang, C. J. A Synthetic Light-Driven Substrate Channeling System for Precise Regulation of Enzyme Cascade Activity Based on DNA Origami. *J. Am. Chem. Soc.* **2018**, *140*, 8990−8996.
(30) Sommese, R. F.; Hariadi, R. F.; Kim, K.; Liu, M.; Tyska, M. J.; Sivaramakrishnan, S. Patterning protein complexes on DNA nanostructures using a GFP nanobody. *Protein Sci.* **2016**, *25*, 2089−2094.
(31) Bustamante, C.; Alexander, L.; Maciuba, K.; Kaiser, C. M. Single-Molecule Studies of Protein Folding with Optical Tweezers. *Annu. Rev. Biochem.* **2020**, *89*, 443−470.
(32) Yin, F.; Zhao, H.; Lu, S.; Shen, J.; Li, M.; Mao, X.; Li, F.; Shi, J.; Li, J.; Dong, B.; Xue, W.; Zuo, X.; Yang, X.; Fan, C. DNA-framework-based multidimensional molecular classifiers for cancer diagnosis. *Nat. Nanotechnol.* **2023**, *18*, 677−686.
(33) Zhang, P.; Liu, X.; Liu, P.; Wang, F.; Ariyama, H.; Ando, T.; Lin, J.; Wang, L.; Hu, J.; Li, B.; Fan, C. Capturing transient antibody conformations with DNA origami epitopes. *Nat. Commun.* **2020**, *11*, 3114.
(34) Huang, F.; Chen, M.; Zhou, Z.; Duan, R.; Xia, F.; Willner, I. Spatiotemporal patterning of photoresponsive DNA-based hydrogels to tune local cell responses. *Nat. Commun.* **2021**, *12*, 2364.
(35) Winfree, E.; Liu, F. R.; Wenzler, L. A.; Seeman, N. C. Design and self-assembly of two-dimensional DNA crystals. *Nature.* **1998**, *394*, 539−544.
(36) Wei, B.; Dai, M.; Yin, P. Complex shapes self-assembled from single-stranded DNA tiles. *Nature.* **2012**, *485*, 623.
(37) Decanniere, K.; Transue, T. R.; Desmyter, A.; Maes, D.; Muyldermans, S.; Wyns, L. Degenerate interfaces in antigen-antibody complexes. *J. Mol. Biol.* **2001**, *313*, 473−478.
(38) Funke, J. J.; Dietz, H. Placing molecules with Bohr radius resolution using DNA origami. *Nat. Nanotechnol.* **2016**, *11*, 47−52.
(39) Bustamante, C.; Bryant, Z.; Smith, S. B. Ten years of tension: single-molecule DNA mechanics. *Nature.* **2003**, *421*, 423−427.
(40) Jiang, S.; Hong, F.; Hu, H.; Yan, H.; Liu, Y. Understanding the Elementary Steps in DNA Tile-Based Self-Assembly. *ACS Nano* **2017**, *11*, 9370−9381.
(41) Liu, P.; Zhao, Y.; Liu, X.; Sun, J.; Xu, D.; Li, Y.; Li, Q.; Wang, L.; Yang, S.; Fan, C. Charge Neutralization Drives the Shape Reconfiguration of DNA Nanotubes. *Angew. Chem., Int. Ed. Engl.* **2018**, *57*, 5418−5422.
(42) Transue, T. R.; De Genst, E.; Ghahroudi, M. A.; Wyns, L.; Muyldermans, S. Camel single-domain antibody inhibits enzyme by mimicking carbohydrate substrate. *Proteins* **1998**, *32*, 515−522.
(43) Walkey, C. D.; Chan, W. C. Understanding and controlling the interaction of nanomaterials with proteins in a physiological environment. *Chem. Soc. Rev.* **2012**, *41*, 2780−2799.
(44) Chinen, A. B.; Guan, C. M.; Ko, C. H.; Mirkin, C. A. The Impact of Protein Corona Formation on the Macrophage Cellular Uptake and Biodistribution of Spherical Nucleic Acids. *Small.* **2017**, *13*, No. 1603847.
(45) Zhang, W.; Meckes, B.; Mirkin, C. A. Spherical Nucleic Acids with Tailored and Active Protein Coronae. *ACS Cent. Sci.* **2019**, *5*, 1983−1990.

https://doi.org/10.1021/jacsau.3c00492
JACS Au 2023, 3, 2709−2714